IOP PUBLISHING JOURNAL OF PHYSICS: CONDENSED MATTER
J. Phys.: Condens. Matter **24** (2012) 095008 (10pp) doi:10.1088/0953-8984/24/9/095008

Contact mechanics for layered materials with randomly rough surfaces

B N J Persson

IFF, FZ-Jülich, D-52425 Jülich, Germany, EU

Received 8 November 2011, in final form 30 December 2011
Published 3 February 2012
Online at stacks.iop.org/JPhysCM/24/095008

Abstract
The contact mechanics model of Persson is applied to layered materials. We calculate the M function, which relates the surface stress to the surface displacement, for a layered material, where the top layer (thickness d) has different elastic properties than the semi-infinite solid below. Numerical results for the contact area as a function of the magnification are presented for several cases. As an application, we calculate the fluid leak rate for laminated rubber seals.

(Some figures may appear in colour only in the online journal)

1. Introduction

Contact mechanics involving layered materials is very common [1]. Thus most solids have thin surface layers with different properties than the bulk. This is the case for all metals (except gold), which are covered by oxide layers. Most engineering surfaces are painted (typically involving thin polymer coatings) or have surface layers to improve their properties, e.g. thin rubber coatings to improve the wear resistance [2, 3] or to prevent barnacles and mussels from attaching themselves to ships' hulls, reducing drag on the ship [4].

Figure 1 shows the contact between a rigid and rough substrate with a rubber block coated with a thin, elastically stiffer layer. In this case the surface of the block may be able to bend and make contact with the substrate on length scales much longer than the thickness d of the stiff layer. However, because of the stiff coating it cannot bend and follow the roughness on length scales of the order of or smaller than the thickness d. This has many important implications. For example, rubber seals are sometimes coated by a thin ($d \approx 10\ \mu$m) Teflon layers to reduce the friction during sliding. However, the coating usually increase the leak rate because the non-contact channels, which exist in the apparent contact area owing to the surface roughness, will be larger for the Teflon-coated rubber than for the uncoated rubber.

We have recently developed a contact mechanics model for randomly rough surfaces [5–7]. The theory is based on studying how the interfacial stress distribution $P(\sigma, \zeta)$ depends on the magnification ζ (or resolution L/ζ, where L is the linear size of the system) at which the interface is probed. This model is very flexible and can be applied to elastic, viscoelastic and elastoplastic materials, and to surfaces with anisotropic roughness. The theory is valid for arbitrary squeezing pressure, e.g. even at so high pressures that nearly

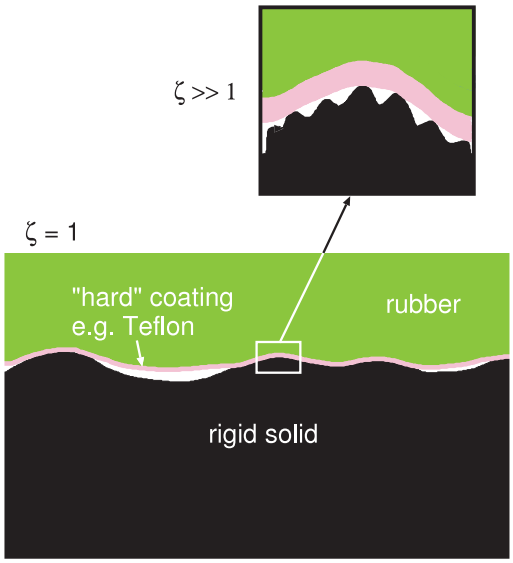

Figure 1. The contact between a rigid and rough substrate with a rubber block coated with a thin, elastically stiffer layer. At low magnification ζ the surface of the block can bend and make contact with the substrate on length scales much longer than the thickness d of the stiff layer. However, at higher magnification it is observed that the surface cannot bend and follow the roughness on length scales of the order of or smaller than the film thickness d.

complete contact prevails (which may be realized only for elastically soft materials such as rubber or gel). Here we will show that the theory can also be applied to layered materials. We first calculate the M function, which relate the surface stress to the surface displacement, for a layered material, where the top layer (thickness d) has different elastic properties than the semi-infinite solid below. Numerical results for the contact area as a function of the magnification are presented for several cases. As an application, we calculate the fluid leak rate for laminated rubber seals with Teflon-like coating.

A large number of papers have been published on contact mechanics for layered materials [8–12]. Thus Bufler has presented a general theory of elasticity for multilayered materials [8]. Burminster studied the deformation of a two-layer system due to a uniform pressure applied within a circular region [9]. Li and Chou presented the elastic solution of a layered half-space with perfect interfacial bonding under an axisymmetrical compressive loading on the plane surface [10]. The analysis is intended to model the nano-indentation of thin-film coating/substrate systems. Nogi and Kato presented a numerical simulation technique for calculating the pressure distribution and the deformed geometry of an elastic half-space which has a hard surface layer in contact with a rigid indenter with a rough surface [11]. Sullivan and King studied the quasi-static sliding contact stress field due to a spherical indenter on an elastic half-space with a single layer [12]. The resulting stresses were discussed for different values of the layer stiffness relative to the substrate and also for different values of the friction coefficient. In [12] the M function was derived in the static limit $\omega = 0$ using the Papkovich–Neuber elastic potential. In this paper we derive the M function for finite frequencies which is relevance in some applications, e.g. rubber sliding friction on layered materials at high sliding velocity [5]. When $\omega \to 0$ our expression for M reduces to that of Sullivan and King. Our method of the derivation of the M function differ from that of [12] and is more general (finite frequencies).

2. Basic equations

Consider the layered material shown in figure 2. Introduce a coordinate system xyz and assume that the z axis is pointing into the solid as indicated in the figure. Let $\boldsymbol{\sigma}$ (a vector with the components σ_i, $i = 1$–3) be the force per unit area (or stress) acting on the surface $z = 0$ and $\mathbf{u}$ the surface displacement induced by σ_i. Let $\mathbf{x} = (x, y)$ and $\mathbf{q} = (q_x, q_y)$ be two-dimensional vectors and write

$$\mathbf{u}(\mathbf{x}, t) = \mathbf{u}(\mathbf{q}, \omega)\mathrm{e}^{\mathrm{i}(\mathbf{q}\cdot\mathbf{x}-\omega t)},$$
$$\boldsymbol{\sigma}(\mathbf{x}, t) = \boldsymbol{\sigma}(\mathbf{q}, \omega)\mathrm{e}^{\mathrm{i}(\mathbf{q}\cdot\mathbf{x}-\omega t)},$$

then

$$\mathbf{u}(\mathbf{q}, \omega) = M(\mathbf{q}, \omega)\boldsymbol{\sigma}(\mathbf{q}, \omega).$$

We define $M(\mathbf{q}) = M(\mathbf{q}, 0)$.

In the Persson contact mechanics model the area of contact (projected on the xy plane) $A(\zeta)$ at the magnification

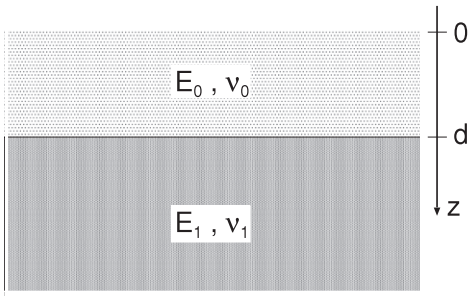

Figure 2. Semi-infinite elastic solid (Young's modulus E_1, Poisson ratio ν_1) with an elastic slab (E_0, ν_0) of thickness d as top layer.

ζ is given by [5]

$$\frac{A(\zeta)}{A_0} = \frac{2}{\sqrt{\pi}}\int_0^{\sqrt{G/2}} \mathrm{d}x\, \mathrm{e}^{-x^2} = \mathrm{erf}\left(\frac{1}{2\sqrt{G}}\right)$$

where A_0 is the nominal contact area and

$$G(\zeta) = \pi\int_{q_0}^{\zeta q_0} \mathrm{d}q\, q|\sigma_0 M_{zz}(q)|^{-2}C(q).$$

In this expression σ_0 is the external squeezing pressure and M_{zz} is the zz component of the matrix $M(\mathbf{q})$.

We now calculate the M function for a layered system consisting of an elastic slap on top of a semi-infinite elastic substrate. Both materials are described as an isotropic elastic continuum. Let $\mathbf{n}$ be a unit vector along the z axis. Following appendix A in [5] we write the elastic deformation field $\mathbf{u}(\mathbf{x}, z, t)$ as

$$\mathbf{u} = \mathbf{p}A + \mathbf{K}B + \mathbf{p}\times\mathbf{K}C \tag{1}$$

where $\mathbf{p} = -\mathrm{i}\nabla$ and $\mathbf{K} = \mathbf{n}\times\mathbf{p}$. In what follows we will assume that all fields depend on $\mathbf{x} = (x, y)$ and on time t as $\exp(\mathrm{i}\mathbf{q}\cdot\mathbf{x} - \mathrm{i}\omega t)$, and we will not write out this $(\mathbf{x}, t)$ dependency explicitly. We have

$$\mathbf{p}\times\mathbf{K} = \mathbf{n}q^2 - \mathbf{q}p_z$$

so that

$$\mathbf{u} = \mathbf{K}B + \mathbf{q}(A - p_z C) + \mathbf{n}(p_z A + q^2 C). \tag{2}$$

Assume that on the surface $z = 0$ act the stress $\sigma_i = \sigma_{3i}$ which we denote as $\boldsymbol{\sigma}$. One can show that for $z = 0$ (see (A12)–(A14) in [5])

$$R_0 A + 2q^2 p_z C = -\frac{\mathrm{i}}{\mu_0}\mathbf{n}\cdot\boldsymbol{\sigma} \tag{3}$$

$$q^2 p_z B = -\frac{\mathrm{i}}{\mu_0}\mathbf{K}\cdot\boldsymbol{\sigma} \tag{4}$$

$$2q^2 p_z A - q^2 R_0 C = -\frac{\mathrm{i}}{\mu_0}\mathbf{q}\cdot\boldsymbol{\sigma} \tag{5}$$

where

$$R_0 = \left(\frac{\omega}{c_{T0}}\right)^2 - 2q^2 \tag{6}$$

where $\mu_0 = E_0/2(1 + \nu_0)$ is the shear modulus and $c_{T0} = (\mu_0/\rho_0)^{1/2}$ is the sound velocity of transverse polarized elastic waves for solid 0 (top layer).

3. *M* function for the *B* field

The *B*-field contribution to $\mathbf{u}$ is denoted by $\mathbf{u}_B$ and is defined by

$$\mathbf{u}_B = \mathbf{K}B \tag{7}$$

where

$$B = B_0(e^{ip_{T0}z} + r_B e^{-ip_{T0}z}) \qquad \text{for } 0 < z < d \tag{8}$$

$$B = B_0 t_B e^{ip_{T1}z} \qquad \text{for } d < z \tag{9}$$

where

$$p_{T0} = \left[\left(\frac{\omega}{c_{T0}}\right)^2 - q^2\right]^{1/2}$$

and similar for p_{T1}. For $z = 0$ we have from (4)

$$q^2 p_z B = -\frac{i}{\mu_0}\mathbf{K}\cdot\boldsymbol{\sigma} \tag{10}$$

and using (8) this gives

$$B_0 = -\frac{i}{\mu_0}\frac{1}{q^2 p_{T0}(1 - r_B)}\mathbf{K}\cdot\boldsymbol{\sigma}. \tag{11}$$

Using (7), (8) and (11) gives for $z = 0$:

$$\mathbf{u}_B = -\frac{i}{\mu_0}\frac{1}{q^2 p_{T0}}\frac{1 + r_B}{1 - r_B}\mathbf{K}\mathbf{K}\cdot\boldsymbol{\sigma}$$

where now $\mathbf{K} = \mathbf{n}\times\mathbf{q}$. Thus if we define $\mathbf{u}_B = M_B\cdot\boldsymbol{\sigma}$ then we can write

$$M_B = -\frac{i}{\mu_0}\frac{1}{q^2 p_{T0}}\frac{1 + r_B}{1 - r_B}\mathbf{K}\mathbf{K}. \tag{12}$$

For $z = d$ both B and $\mu p_z B$ must be continuous. This gives

$$e^{ip_{T0}d} + r_B e^{-ip_{T0}d} = t_B e^{ip_{T1}d} \tag{13}$$

$$\mu_0 p_{T0}(e^{ip_{T0}d} - r_B e^{-ip_{T0}d}) = \mu_1 p_{T1} t_B e^{ip_{T1}d}. \tag{14}$$

Thus

$$\frac{1 - r_B e^{-i2p_{T0}d}}{1 + r_B e^{-i2p_{T0}d}} = \frac{\mu_1 p_{T1}}{\mu_0 p_{T0}} \tag{15}$$

or

$$r_B = \frac{\mu_0 p_{T0} - \mu_1 p_{T1}}{\mu_0 p_{T0} + \mu_1 p_{T1}} e^{i2p_{T0}d}. \tag{16}$$

Substituting this in (12) gives $M_B(q, \omega)$.

In the limit $\omega \to 0$ we get

$$p_{T0} = \left[\left(\frac{\omega}{c_{T0}}\right)^2 - q^2\right]^{1/2} \to iq \tag{17}$$

and similar for p_{T1} so that

$$r_B \approx \frac{\mu_0 - \mu_1}{\mu_0 + \mu_1} e^{-2qd} \tag{18}$$

and

$$\frac{1 + r_B}{1 - r_B} \approx \frac{(\mu_0 + \mu_1) + (\mu_0 - \mu_1)e^{-2qd}}{(\mu_0 + \mu_1) - (\mu_0 - \mu_1)e^{-2qd}}. \tag{19}$$

Substituting this in (12) gives $M_B(q) = M_B(q, 0)$:

$$M_B(q) = -\frac{1}{\mu_0 q^3}\frac{(\mu_0 + \mu_1) + (\mu_0 - \mu_1)e^{-2qd}}{(\mu_0 + \mu_1) - (\mu_0 - \mu_1)e^{-2qd}}\mathbf{K}\mathbf{K}. \tag{20}$$

If we introduce the unit vector $\mathbf{e} = \hat{z}\times\hat{q}$ we can also write

$$M_B(q) = -\frac{1}{\mu_0 q}\frac{(\mu_0 + \mu_1) + (\mu_0 - \mu_1)e^{-2qd}}{(\mu_0 + \mu_1) - (\mu_0 - \mu_1)e^{-2qd}}\mathbf{e}\mathbf{e}. \tag{21}$$

When $\mu_0 = \mu_1$ we get $M_B = (1/\mu_0 q)\mathbf{e}\mathbf{e}$ which is a well-known result (see the appendix in [13]).

4. *M* function for the *A* and *C* fields

The M function for the A and C fields is much more complicated to calculate in part because these fields are coupled at the interfaces and also because we need to calculate $r_A(\omega)$ and $r_C(\omega)$ to first order in $(\omega/cq)^2$ even if we are just interested in $M(\mathbf{q}, \omega)$ for $\omega = 0$ (see below).

In what follows we will assume that the stress $\boldsymbol{\sigma}$ is normal to the surface $z = 0$ and we will only focus on the z component of $\mathbf{u}$. From (2)

$$u_z = p_z A + q^2 C \tag{22}$$

and (3) and (5) reduces to

$$R_0 A + 2q^2 p_z C = -\frac{i}{\mu_0}\mathbf{n}\cdot\boldsymbol{\sigma} \tag{23}$$

$$2p_z A - R_0 C = 0. \tag{24}$$

The last equation gives $p_z A = R_0 C/2$ so that for $z = 0$

$$u_z = p_z A + q^2 C = \frac{1}{2}(R_0 C + 2q^2 C) = \frac{1}{2}\left(\frac{\omega}{c_{T0}}\right)^2 C. \tag{25}$$

This equation shows that, in order for u_z to be finite as $\omega \to 0$, it is necessary that $C \sim \omega^{-2}$ as $\omega \to 0$.

Let us write

$$A = A_0(e^{ip_{L0}z} + r_A e^{-ip_{L0}z}) \qquad \text{for } 0 < z < d \tag{26}$$

$$C = C_0(e^{ip_{T0}z} + r_C e^{-ip_{T0}z}) \qquad \text{for } 0 < z < d \tag{27}$$

$$A = A_0 t_A e^{ip_{L1}z} \qquad \text{for } d < z \tag{28}$$

$$C = C_0 t_C e^{ip_{T1}z} \qquad \text{for } d < z. \tag{29}$$

Substituting this in (23) and (24) gives

$$R_0 A_0(1 + r_A) + 2q^2 p_{T0} C_0(1 - r_C) = -\frac{i}{\mu_0}\mathbf{n}\cdot\boldsymbol{\sigma} \tag{30}$$

$$2p_L A_0(1 - r_A) - R_0 C_0(1 + r_C) = 0. \tag{31}$$

Using (30) and (31):

$$C_0(1 + r_C) = -\frac{i}{\mu_0}\frac{2p_{L0}\sigma_z}{R_0^2 Z_A + 4q^2 p_{L0} p_{T0} Z_C} \tag{32}$$

where

$$Z_A = \frac{1 + r_A}{1 - r_A}, \qquad Z_C = \frac{1 - r_C}{1 + r_C}. \tag{33}$$

Using (25) this gives

$$u_z = M_{zz}\sigma_z \tag{34}$$

with

$$M_{zz} = \frac{1}{\mu_0}\left(\frac{\omega}{c_T}\right)^2 \frac{2q}{R_0^2 Z_A + 4q^2 p_{L0} p_{T0} Z_C}. \tag{35}$$

Note that as $\omega \to 0$ we have $R_0^2 \to 4q^4$ and $4q^2 p_{L0} p_{T0} \to -4q^2$. Thus in order for M_{zz} to remain non-zero as $\omega \to 0$ we must have $Z_A = Z_C$ for $\omega = 0$. We can expand

$$Z_A(\omega) = a_0 + a_1\left(\frac{\omega}{c_{L0}q}\right)^2 \tag{36}$$

$$Z_C(\omega) = c_0 + c_1\left(\frac{\omega}{c_{T0}q}\right)^2 \tag{37}$$

where $a_0 = c_0$. Substituting (36) and (37) in (35) gives $M_{zz}(q) = M_{zz}(q, 0)$:

$$M_{zz}(q) = \frac{1}{\mu_0 q}\frac{1}{[(c_{T0}/c_{L0})^2 - 1]a_0 + 2[a_1 (c_{T0}/c_{L0})^2 - c_1]}$$

or

$$M_{zz}(q) = -\frac{2(1-\nu_0^2)}{E_0 q}S(q) = -\frac{2}{E_0^* q}S(q) \tag{38}$$

where $E_0^* = E_0/(1-\nu_0^2)$ and where

$$S(q) = \frac{(c_{T0}/c_{L0})^2 - 1}{[(c_{T0}/c_{L0})^2 - 1]a_0 + 2[a_1 (c_{T0}/c_{L0})^2 - c_1]}. \tag{39}$$

Using that

$$\left[\left(\frac{c_{T0}}{c_{L0}}\right)^2 - 1\right]^{-1} = -2(1-\nu_0) \tag{40}$$

and

$$\left(\frac{c_{T0}}{c_{L0}}\right)^2\left[\left(\frac{c_{T0}}{c_{L0}}\right)^2 - 1\right]^{-1} = -(1-2\nu_0) \tag{41}$$

we get from (39)

$$S(q) = \frac{1}{a_0 - a_1 2(1-2\nu_0) + c_1 4(1-\nu_0)}. \tag{42}$$

For a semi-infinite solid (no layer system) $r_A = r_C = 0$ so that $a_0 = 1$, $a_1 = c_1 = 0$ and (42) reduces to $S = 1$.

If we expand the reflection factors

$$r_A(\omega) = a_0' + a_1'\left(\frac{\omega}{c_{L0}q}\right)^2 \tag{43}$$

$$r_C(\omega) = c_0' + c_1'\left(\frac{\omega}{c_{T0}q}\right)^2 \tag{44}$$

then we can write

$$a_0 = \frac{1+a_0'}{1-a_0'}, \qquad a_1 = \frac{2a_1'}{(1-a_0')^2} \tag{45}$$

$$c_0 = \frac{1-c_0'}{1+c_0'}, \qquad c_1 = \frac{-2c_1'}{(1+c_0')^2}. \tag{46}$$

Note also that $a_0 = c_0$ implies that $a_0' = -c_0'$. Substituting (45) and (46) in (42) gives

$$S(q) = \frac{(1-a_0')^2}{1 - a_0'^2 - 4a_1'(1-2\nu_0) - 8c_1'(1-\nu_0)}. \tag{47}$$

4.1. M_{zz} for a limiting case

We consider first a simple limiting case, namely where the solid for $z > d$ can be considered as rigid and where there is no friction between the elastic slab and the substrate. In this case $u_z = 0$ and $\sigma_\parallel = 0$ for $z = d$. From (5) it follows that the parallel stress will vanish for $z = d$ if $2p_z A + R_0 C = 0$ for $z = d$, while from (2) it follows that u_z will vanish for $z = d$ if $p_z A + q^2 C = 0$ for $z = d$. Thus we conclude that $C = 0$ and $p_z A = 0$ for $z = d$. This gives

$$e^{ip_{T0}d} + r_C e^{-ip_{T0}d} = 0 \tag{48}$$

$$e^{ip_{L1}d} - r_A e^{-ip_{L1}d} = 0. \tag{49}$$

Thus

$$Z_A = \frac{1 + e^{2ip_{L1}d}}{1 - e^{2ip_{L1}d}}, \qquad Z_C = \frac{1 + e^{2ip_{T1}d}}{1 - e^{2ip_{T1}d}}.$$

Substituting these results in (35) gives $M_{zz}(q, \omega)$.

In the limit $\omega \to 0$ we can expand

$$r_C = -e^{i2p_{T0}d} \approx -e^{-2qd}\left[1 + qd\left(\frac{\omega}{c_{T0}q}\right)^2\right] \tag{50}$$

$$r_A = e^{i2p_{L0}d} \approx e^{-2qd}\left[1 + qd\left(\frac{\omega}{c_{L0}q}\right)^2\right]. \tag{51}$$

Thus

$$a_0' = -c_0' = e^{-2qd} \tag{52}$$

and

$$a_1' = -c_1' = e^{-2qd}qd. \tag{53}$$

Substituting these results in (47) gives

$$S(q) = \frac{1}{a_0 + 2a_1} = \frac{(1 - e^{-2qd})^2}{1 - e^{-4qd} + 4qde^{-2qd}}. \tag{54}$$

Note that $S \to 1$ as $qd \to \infty$.

4.2. M_{zz} for the general case

The displacement field **u** and the stress must be continuous for $z = d$. The continuity of **u** implies that $A - p_z C$ and $p_z A + q^2 C$ must be continuous for $z = d$. The continuity of the stress implies that $\mu(RA + 2q^2 p_z C)$ and $\mu(2p_z A - RC)$ (where $R = R_0$ for $z < d$ and $R = R_1$ for $z > d$, where R_1 is obtained by replacing c_{T0} with c_{T1} in the expression for R_0) are continuous. It is convenient to write $\mu(RA + 2q^2 p_z C) = \mu[(R+2q^2)A - 2q^2(A - p_z C)]$ and $\mu(2p_z A - RC) = \mu[2(p_z A + q^2 C) - (R + 2q^2)C]$ since the bracket terms involving p_z are continuous in both cases. Note that $(R + 2q^2) = (\omega/c_T)^2 =$

κ is already of order ω^2. Using (26)–(29) and denoting $\alpha = p_{T0}C_0/A_0$ the continuity of **u** implies

$$U_1 = T_A - \alpha\frac{p_{T1}}{p_{T0}}T_C \tag{55}$$

$$U_2 = \frac{p_{L1}}{p_{L0}}T_A + \frac{\alpha q^2}{p_{T0}p_{L0}}T_C \tag{56}$$

where

$$U_1 = (e^{ip_{L0}d} + r_A e^{-ip_{L0}d}) - \alpha\left(e^{ip_{T0}d} - r_C e^{-ip_{T0}d}\right) \tag{57}$$

$$U_2 = (e^{ip_{L0}d} - r_A e^{-ip_{L0}d}) + \frac{\alpha q^2}{p_{T0}p_{L0}} \times (e^{ip_{T0}d} + r_C e^{-ip_{T0}d}) \tag{58}$$

$$T_A = t_A e^{ip_{L1}d}, \qquad T_C = t_C e^{ip_{T1}d}. \tag{59}$$

The continuity of the stress gives

$$\mu_0\kappa_0(e^{ip_{L0}d} + r_A e^{-ip_{L0}d}) - (\mu_0 - \mu_1)2q^2U_1 = \mu_1\kappa_1 T_A$$

or

$$T_A = \frac{\mu_0\kappa_0}{\mu_1\kappa_1}(e^{ip_{L0}d} + r_A e^{-ip_{L0}d}) - \frac{2(\mu_0 - \mu_1)}{\mu_1\kappa_1}q^2U_1 \tag{60}$$

and

$$\frac{\mu_0\kappa_0\alpha}{p_{T0}p_{L0}}(e^{ip_{T0}d} + r_C e^{-ip_{T0}d}) - (\mu_0 - \mu_1)2U_2 = \frac{\mu_1\kappa_1\alpha}{p_{T0}p_{L0}}T_C$$

or

$$T_C = \frac{\mu_0\kappa_0}{\mu_1\kappa_1}(e^{ip_{T0}d} + r_C e^{-ip_{T0}d}) - \frac{2(\mu_0 - \mu_1)}{\mu_1\kappa_1}\frac{p_{T0}p_{L0}}{\alpha}U_2. \tag{61}$$

Using (31) we have

$$\alpha = \frac{2p_{T0}p_{L0}(1 - r_A)}{R_0(1 + r_C)}. \tag{62}$$

Equations (55)–(62) constitute five equations for five unknowns $(r_A, t_A, r_C, t_C, \alpha)$. To zero order in ω^2 the equations above are all satisfied if $r_A(0) = -r_C(0)$ (or $a_0' = -c_0'$) and $t_A(0) = t_C(0)$. Note that $\alpha \to 1$ as $\omega \to 0$.

From (55) and (56) we get

$$U_2 - \frac{p_{L1}}{p_{L0}}U_1 = \frac{\alpha(q^2 + p_{T1}p_{L1})}{p_{T0}p_{L0}}T_C \tag{63}$$

$$\frac{p_{T1}}{p_{T0}}U_2 + \frac{q^2}{p_{T0}p_{L0}}U_1 = \frac{(q^2 + p_{T1}p_{L1})}{p_{T0}p_{L0}}T_A. \tag{64}$$

Substituting (60) and (61) in (63) and (64) and defining $\phi(\omega) = (q^2 + p_{T1}p_{L1})/\kappa_1$ gives

$$U_2 - \frac{p_{L1}}{p_{L0}}U_1 = \frac{\phi\mu_0\kappa_0\alpha}{\mu_1 p_{T0}p_{L0}}(e^{ip_{T0}d} + r_C e^{-ip_{T0}d}) - \frac{2\phi(\mu_0 - \mu_1)}{\mu_1}U_2$$

$$\frac{p_{T1}}{p_{T0}}U_2 + \frac{q^2}{p_{T0}p_{L0}}U_1 = \frac{\phi\mu_0\kappa_0}{\mu_1 p_{T0}p_{L0}}(e^{ip_{L0}d} + r_A e^{-ip_{L0}d}) - \frac{2\phi(\mu_0 - \mu_1)q^2}{\mu_1 p_{T0}p_{L0}}U_1$$

or

$$-\frac{p_{L1}}{p_{L0}}U_1 + \left(1 + \frac{2\phi(\mu_0 - \mu_1)}{\mu_1}\right)U_2 = \frac{\phi\mu_0\kappa_0\alpha}{\mu_1 p_{T0}p_{L0}}(e^{ip_{T0}d} + r_C e^{-ip_{T0}d}) \tag{65}$$

$$\frac{q^2}{p_{T0}p_{L0}}\left(1 + \frac{2\phi(\mu_0 - \mu_1)}{\mu_1}\right)U_1 + \frac{p_{T1}}{p_{T0}}U_2 = \frac{\phi\mu_0\kappa_0}{\mu_1 p_{T0}p_{L0}}(e^{ip_{L0}d} + r_A e^{-ip_{L0}d}). \tag{66}$$

Substituting (57) and (58) in (65) and (66) gives

$$a_{11}r_A + a_{12}r_C = b_1$$
$$a_{21}r_A + a_{22}r_C = b_2$$

or

$$r_A = \frac{a_{22}b_1 - a_{12}b_2}{a_{11}a_{22} - a_{12}a_{21}} \tag{67}$$

$$r_C = \frac{a_{11}b_2 - a_{21}b_1}{a_{11}a_{22} - a_{12}a_{21}} \tag{68}$$

where

$$a_{11} = -\left(\frac{p_{L1}}{p_{L0}} + \psi\right)e^{-ip_{L0}d} \tag{69}$$

$$a_{12} = -\alpha\left(\frac{p_{L1}}{p_{L0}} - \frac{\psi q^2}{p_{T0}p_{L0}} + \frac{\phi\mu_0\kappa_0}{\mu_1 p_{T0}p_{L0}}\right)e^{-ip_{T0}d} \tag{70}$$

$$a_{21} = \left(\frac{\psi q^2}{p_{T0}p_{L0}} - \frac{\phi\mu_0\kappa_0}{\mu_1 p_{T0}p_{L0}} - \frac{p_{T1}}{p_{T0}}\right)e^{-ip_{L0}d} \tag{71}$$

$$a_{22} = \alpha\left(\frac{\psi q^2}{p_{T0}p_{L0}} + \frac{p_{T1}}{p_{T0}}\frac{q^2}{p_{T0}p_{L0}}\right)e^{-ip_{T0}d} \tag{72}$$

$$b_1 = \alpha\left(\frac{\phi\mu_0\kappa_0}{\mu_1 p_{T0}p_{L0}} - \frac{p_{L1}}{p_{L0}} - \frac{\psi q^2}{p_{T0}p_{L0}}\right)e^{ip_{T0}d} + \left(\frac{p_{L1}}{p_{L0}} - \psi\right)e^{ip_{L0}d} \tag{73}$$

$$b_2 = \alpha\left(\frac{\psi q^2}{p_{T0}p_{L0}} - \frac{p_{T1}}{p_{T0}}\frac{q^2}{p_{T0}p_{L0}}\right)e^{ip_{T0}d} + \left(\frac{\phi\mu_0\kappa_0}{\mu_1 p_{T0}p_{L0}} - \frac{\psi q^2}{p_{T0}p_{L0}} - \frac{p_{T1}}{p_{T0}}\right)e^{ip_{L0}d} \tag{74}$$

where

$$\psi = 1 + \frac{2\phi(\mu_0 - \mu_1)}{\mu_1}. \tag{75}$$

Using (33), (35) and (67)–(75) gives $M_{zz}(q, \omega)$.

Note that for $\omega = 0$, $a_{11} = a_{22} = a_{12} = a_{22} = -(1 + \psi)e^{qd}$ and $b_1 = b_2 = 0$ so that both the numerator and the denominator in (67) and (68) vanish. Thus it is necessary to include higher-order terms in ω^2 in order to calculate r_A and r_C. Expanding r_A and r_B to order ω^2 and using (47) gives after some simplifications

$$S = \frac{1 + 4mqde^{-2qd} - mne^{-4qd}}{1 - (m + n + 4mq^2d^2)e^{-2qd} + mne^{-4qd}} \tag{76}$$

where

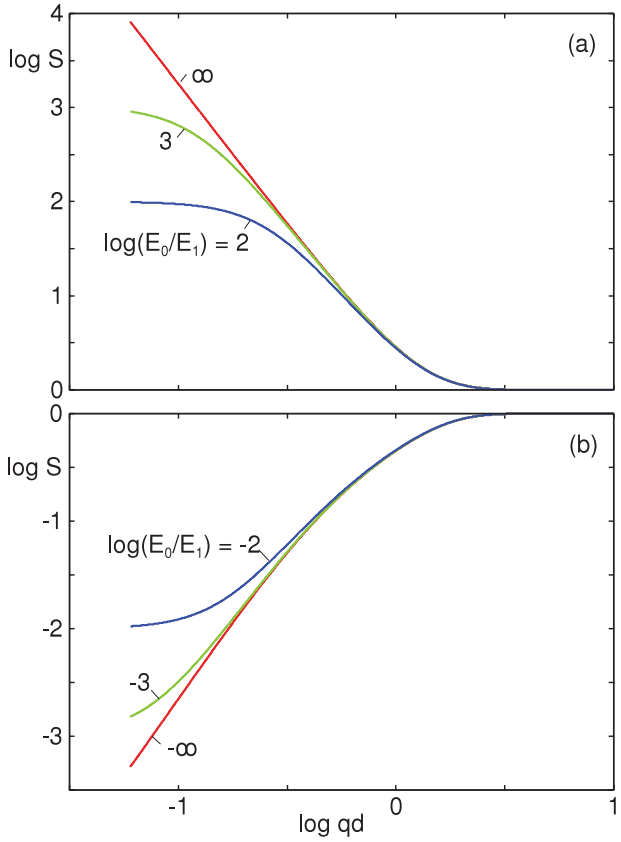

Figure 3. The logarithm of the surface response function S as a function of the logarithm of qd, where q is the wavevector and d the film thickness, for two different cases: (a) stiff layer on top of a soft semi-infinite solid and (b) soft layer on top of a semi-infinite stiff solid. The red curves are results for (a) a free elastic slab and (b) an elastic slab on top of a rigid solid. In both cases the Poisson ratio $\nu_0 = \nu_1 = 0.5$.

$$m = \frac{\mu_0/\mu_1 - 1}{\mu_0/\mu_1 + 3 - 4\nu_0},$$
$$n = 1 - \frac{4(1-\nu_0)}{1 + (\mu_0/\mu_1)(3-4\nu_1)}$$

where the shear modulus $\mu_0 = E_0/2(1+\nu_0)$ and similar for μ_1. Note also that S is dimensionless and only depends on qd, ν_0, ν_1 and E_0/E_1. Equation (76) agree with the result obtained by Sullivan and King [12] using a very different method of derivation limited to $\omega = 0$.

4.3. Two important limiting cases

Two important limits of (76) are (a) a free elastic slab (thickness d) and (b) an elastic slab in contact with a rigid flat surface. The first case corresponds to $E_1 = 0$ and the second to $E_1 = \infty$. For these two cases (67) reduces to [14, 15]

$$S_a = \frac{\sinh(2qd) + 2qd}{\cosh(2qd) - 2\,(qd)^2 - 1} \tag{77}$$

$$S_b = \frac{(3-4\nu_0)\sinh(2qd) - 2qd}{(3-4\nu_0)\cosh(2qd) + 2\,(qd)^2 - 4\nu_0(3-4\nu_0) + 5}. \tag{78}$$

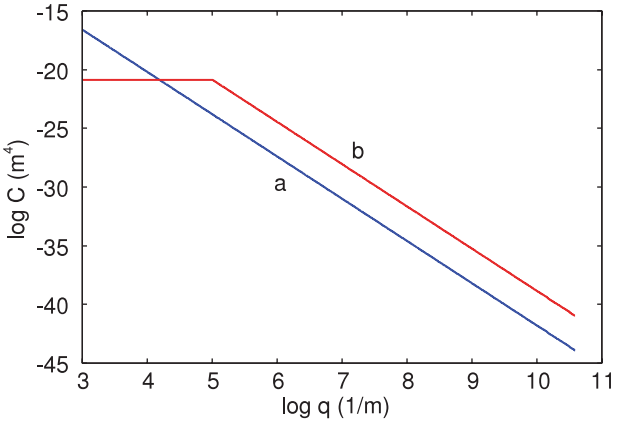

Figure 4. The logarithm of the surface roughness power spectrum C as a function of the logarithm of the wavevector q for two surfaces with the root-mean-square roughness 10 μm and the large and small wavevector cutoff $q_1 = 3.9 \times 10^{10}$ m^{-1} and $q_0 = 10^3$ m^{-1}. Curve **b** is with the roll-off wavevector $q_r = 10^5$ m^{-1} while in case **a** there is no roll-off. For $q_r < q < q_1$ the surface is self-affine fractal with the fractal dimension $D_f = 2.2$ (corresponding to the Hurst exponent $H = 0.8$).

In figure 3 we shows the logarithm of the surface response function S as a function of the logarithm of qd, where q is the wavevector and d is the film thickness, for two different cases: (a) stiff layer on top of a soft semi-infinite solid and (b) soft layer on top of a semi-infinite stiff solid. The red curves are the analytical results for (a) a free elastic slab and (b) an elastic slab on top of a rigid solid. In both cases the Poisson ratio $\nu_0 = \nu_1 = 0.5$. As expected, for $qd \ll 1$ the M response function is determined by the bulk properties of the layered material so that $S \to E_0^*/E_1^*$ as $qd \to 0$. However, when $qd \to \infty$ only the top layer determine the M function so that $S \to 1$ in this limiting case.

Note that bending effects are fully taken into account in the theory presented above, since the derivation is based on the Navier equation of motion of an elastic body, which is the foundation of the theory of elasticity and therefore of also, in particular, for the theory of the bending of plates. As an example if one considers a free elastic plate described by equation (77) it is clear that for small values of qd one exactly gets the solution for pure bending of plates. Thus if we assume $qd \ll 1$ and expand both the numerator and denominator in (77) to leading order in qd we get $S_a = 6/(qd)^3$. Substituting this into the definition $M_{zz} = -2S(q)/(E^*q)$ gives $M_{zz} = -12/(E^*q^4d^3)$. This is exactly the result obtained from the theory of the bending of plates, where the normal displacement u satisfies $D\nabla^2\nabla^2 u = -\sigma$ or, after Fourier transformation, $u(q) = -\sigma(q)/(Dq^4)$, where the bending stiffness $D = E^*d^3/12$. This is identical to the prediction of (77) for $qd \ll 1$.

5. Numerical results

In what follows we will present numerical results for two surfaces **a** and **b**, with the power spectra shown in figure 4. Both surfaces have the root-mean-square roughness 10 μm

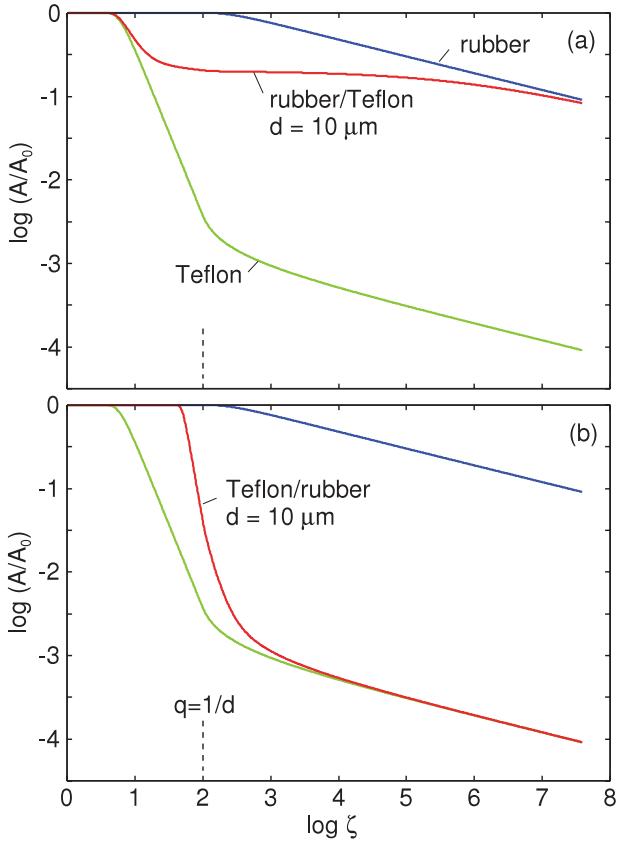

Figure 5. The logarithm (with 10 as the base) of the (normalized) contact area as a function of the logarithm of the magnification for (a) a $d = 10$ μm thick rubber film (elastic modulus $E_0 = 10^6$ Pa, Poisson ratio $\nu_0 = 0.5$) on top of a semi-infinite Teflon solid (elastic modulus $E_1 = 10^9$ Pa, Poisson ratio $\nu_1 = 0.5$) and (b) for the reversed system Teflon on rubber. The squeezing pressure $p = 1$ MPa and the surface roughness power spectra given by curve **b** in figure 4.

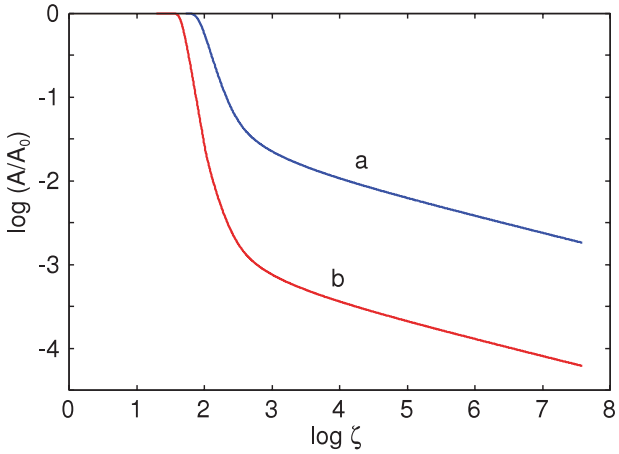

Figure 6. The logarithm (with 10 as the base) of the (normalized) contact area as a function of the logarithm of the magnification for a $d = 10$ μm thick Teflon film (elastic modulus $E_1 = 10^9$ Pa, Poisson ratio $\nu_1 = 0.5$) on top of a semi-infinite rubber solid (elastic modulus $E_0 = 10^6$ Pa, Poisson ratio $\nu_0 = 0.5$). The two curves **a** and **b** are for the two power spectra **a** and **b** in figure 4. The squeezing pressure $p = 1$ MPa.

and the large and small wavevector cutoff $q_1 = 3.9 \times 10^{10}$ m^{-1} and $q_0 = 10^3$ m^{-1}. Curve **b** is with the roll-off wavevector $q_r = 10^5$ m^{-1} while in case **a** there is no roll-off. For $q_r < q < q_1$ the surfaces are self-affine fractal with the fractal dimension $D_f = 2.2$ (corresponding to the Hurst exponent $H = 0.8$). Note that the rms roughness h_{rms} is mainly determined by the longest wavelength roughness, while the area of real contact is determined mainly by the short-wavelength roughness. It is interesting to note that, for $q > q_r$, the power spectra $C(q)$ for surface **b** is ∼1000 times larger than for surface **a**, in spite of the fact that the two surfaces have the same rms roughness value. This has important implications for the leak rate of seals (see below).

5.1. Contact area

In figure 5 we show for surface **b** the logarithm (with 10 as the base) of the (normalized) contact area as a function of the logarithm of the magnification. Figure 5(a) is for a $d = 10$ μm thick rubber film (elastic modulus $E_0 = 10^6$ Pa, Poisson ratio $\nu_0 = 0.5$) on top of a stiffer semi-infinite solid (elastic modulus $E_1 = 10^9$ Pa, Poisson ratio $\nu_1 = 0.5$), which we will refer to as Teflon, and (b) for the reversed system with Teflon film on rubber. The vertical dashed line indicates the magnification where $q = \zeta q_0 = 1/d$. Also shown in the figure is the result obtained with only rubber (blue curve) and only Teflon (green curve). Note that for large magnification the contact area is given by the properties of the top layer. In what follows we will focus on case (b) with Teflon film on rubber. Real Teflon has similar elastic properties as we use above but a rather small penetration hardness (about 30 MPa) and will yield plastically already at rather low contact stresses. However, as we will argue below, this does not affect the leak rate of Teflon-coated rubber seals (see section 5.2) and we will neglect plastic yielding in most of the calculations in order to more clearly exhibit the basic physics involved in the contact mechanics for laminated systems.

In figure 6 we show the logarithm (with 10 as the base) of the (normalized) contact area as a function of the logarithm of the magnification for a $d = 10$ μm thick Teflon film on top of a semi-infinite rubber solid. The two curves are for the two power spectra **a** and **b** in figure 4. The leak rate is determined mainly by the size of the critical junction observed (during increasing magnification) at the magnification ζ_c, where the first percolating channel appears, i.e. for $A(\zeta_c)/A_0 \approx 0.5$. At the squeezing pressure used in figure 6 ($p = 1$ MPa) we get $\zeta_c \approx 70$ and ≈100 for surfaces **b** and **a**, respectively. This correspond to the wavevectors $q = \zeta_c q_0 \approx 7 \times 10^4$ and $\approx 10^5$ m^{-1}. Figure 4 shows that for these wavevectors the surface roughness power spectrum is much larger for surface **b** than for surface **a**, and we therefore expect larger leakage for surface **b**.

Teflon has a Poisson ratio $\nu \approx 0.5$ and polymers in general have $0.3 < \nu < 0.5$. In figure 7 we show the logarithm (with 10 as the base) of the (normalized) contact area as a function of the logarithm of the magnification for two $d = 10$ μm thick polymer films with the elastic modulus

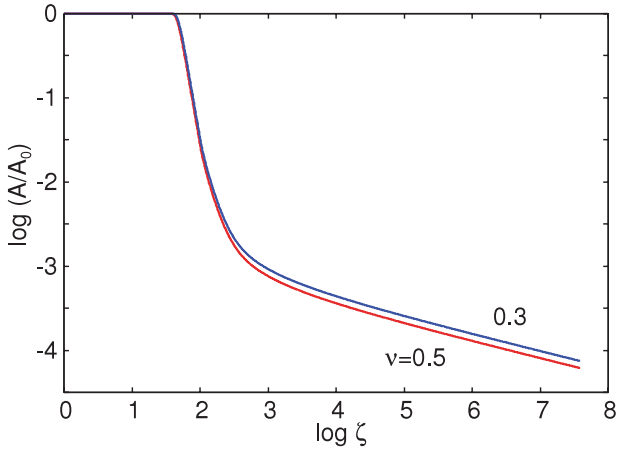

Figure 7. The logarithm (with 10 as the base) of the (normalized) contact area as a function of the logarithm of the magnification for two $d = 10$ μ*m* thick polymer films with the elastic modulus $E_1 = 10^9$ Pa and the Poisson ratio $\nu_1 = 0.5$ and 0.3, on top of a semi-infinite rubber solid (elastic modulus $E_0 = 10^6$ Pa, Poisson ratio $\nu_0 = 0.5$). The curves are for the power spectra **b** in figure 4. The squeezing pressure $p = 1$ MPa.

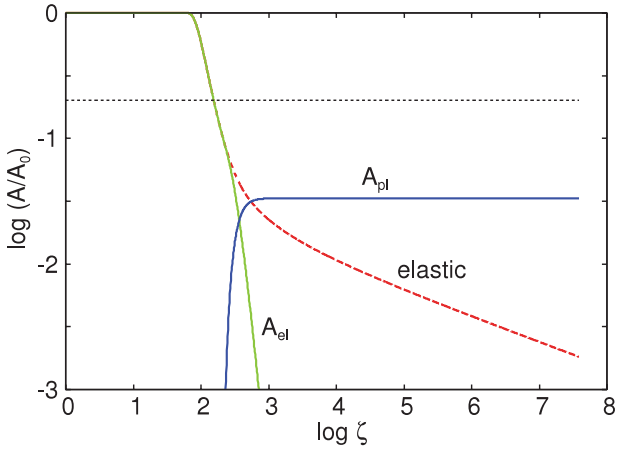

Figure 8. The logarithm (with 10 as the base) of the (normalized) contact area as a function of the logarithm of the magnification for two $d = 10$ μm thick polymer films with the elastic modulus $E_1 = 10^9$ Pa and the Poisson ratio $\nu_1 = 0.5$, on top of a semi-infinite rubber solid (elastic modulus $E_0 = 10^6$ Pa, Poisson ratio $\nu_0 = 0.5$). The dashed curve is for elastic contact (from figure 6), while the blue and green curves are for elastoplastic contact with the penetration hardness 30 MPa. The blue curve is the contact area which has yielded plastically and the green curve the elastic contact area. The horizontal dotted line corresponds to $A/A_0 = 0.5$. The curves are for the power spectra **a** in figure 4. The squeezing pressure $p = 1$ MPa.

$E_1 = 10^9$ Pa and the Poisson ratio $\nu_1 = 0.5$ and 0.3, on top of a semi-infinite rubber solid. In both cases we have assumed the power spectra **b** in figure 4. Note that the contact area depends only weakly on the Poisson ratio.

Figure 8 shows the logarithm of the (normalized) contact area as a function of the logarithm of the magnification for two $d = 10$ μ*m* thick polymer films with the elastic modulus $E_1 = 10^9$ Pa and the Poisson ratio $\nu_1 = 0.5$, on top of a semi-infinite rubber solid (elastic modulus $E_0 = 10^6$ Pa, Poisson ratio $\nu_0 = 0.5$). The dashed curve is for elastic contact (from figure 6), while the blue and green curves are for elastoplastic contact with the penetration hardness 30 MPa as is typical for Teflon. The blue curve is the contact area which has yielded plastically and the green curve the elastic contact area. The curves are for the power spectra **a** in figure 4.

The horizontal dotted line in figure 8 correspond to $A/A_0 = 0.5$. The condition $A(\zeta)/A_0 \approx 0.5$ determines the point where the non-contact percolates which results in most of the leak rate of seals (see section 5.2). Note that at the magnification when the contact area equals $A/A_0 = 0.5$ plastic deformation is negligible. Thus we can neglect plastic deformation when studying the leak rate for surface **a** squeezed against a flat surface at the (nominal) contact pressure 1 MPa, which is typical for rubber seals.

5.2. Leak rate for laminated rubber seals

Rubber seals, e.g. rubber O-rings, is of great importance in very many mechanical constructions. Because of its low elastic modulus ($E \approx 1$ MPa), already nominal contact pressures of order ∼1 MPa may result in nearly complete contact between a rubber body and the countersurface, e.g. a polished steel surface, resulting in good sealing. However, the friction between the rubber and an unlubricated countersurface can be very high, e.g. the friction coefficient for a rubber–steel contact is typically of order unity, and sometimes even higher. In some applications the confined fluid has a very low viscosity, e.g. for water, and in this case the friction may be very high for all relevant sliding velocities. In such cases it may be useful to coat the rubber surface with a low friction material like Teflon. However, Teflon, and other coating materials, usually have a much higher elastic modulus than rubber which may result in large non-contact (fluid leak) channels at the interface for laminated rubber seals. Here we will show how the theory developed above may be used to study this problem in detail.

In earlier publications we have studied fluid flow at interfaces using the so-called critical junction theory and an effective medium theory [16, 17]. The critical junction theory is accurate at high enough contact pressures, while the effective medium theory holds (approximately) for all contact pressures. Let us first briefly describe the critical junction theory.

Consider the fluid leakage through a rubber seal, from a high fluid pressure P_a region, to a low fluid pressure P_b region. Assume for simplicity that the nominal contact region between the rubber and the hard countersurface is rectangular with area $L \times L$. Now, let us study the contact between the two solids as we change the magnification ζ. We define $\zeta = L/\lambda$, where λ is the resolution. We study how the apparent contact area, $A(\zeta)$, between the two solids depends on the magnification ζ. At the lowest magnification we cannot observe any surface roughness and the contact between the solids appears to be complete i.e. $A(1) = A_0$. As we increase the magnification we will observe some interfacial roughness and the (apparent) contact area will decrease. At high enough magnification, say $\zeta = \zeta_c$, a percolating path of non-contact area will be observed for the first time. The most narrow constriction along the percolation path, which we denote as

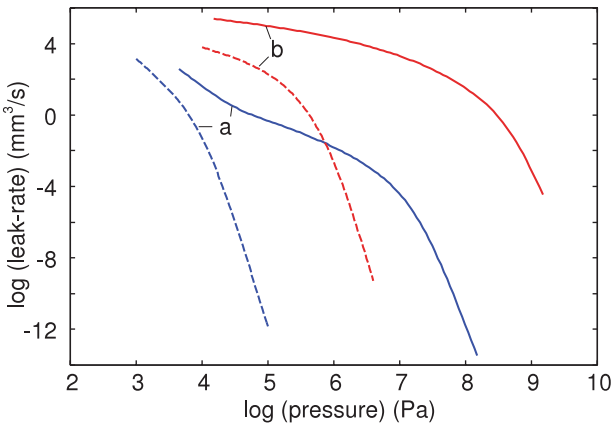

Figure 9. The logarithm (with 10 as the base) of the leak rate as a function of the logarithm of the squeezing pressure for a $d = 10$ μm thick Teflon film (elastic modulus $E_1 = 10^9$ Pa, Poisson ratio $\nu_1 = 0.5$) on top of a semi-infinite rubber solid (elastic modulus $E_0 = 10^6$ Pa, Poisson ratio $\nu_0 = 0.5$). The results are for the power spectra **a** and **b** in figure 4 and for the (Teflon) laminated rubber (solid lines) and for pure rubber (dashed lines). The fluid viscosity $\eta = 0.001$ Pa s and the fluid pressure drop $\Delta P = 0.1$ MPa. We have assumed the ratio $L_x/L_y = 16$.

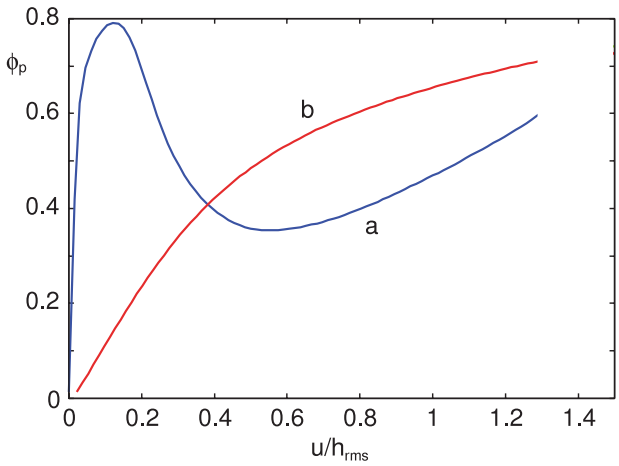

Figure 10. The pressure flow factor ϕ_p as a function of the average interfacial separation for a $d = 10$ μm thick Teflon film (elastic modulus $E_1 = 10^9$ Pa, Poisson ratio $\nu_1 = 0.5$) on top of a semi-infinite rubber block (elastic modulus $E_0 = 10^6$ Pa, Poisson ratio $\nu_0 = 0.5$). The results are for the power spectra **a** and **b** in figure 4.

the critical constriction, will have the lateral size $\lambda_c = L/\zeta_c$ and the surface separation at this point is denoted by $u_c = u_1(\zeta_c)$, and is given by the Persson contact mechanics theory. As we continue to increase the magnification we will find more percolating channels between the surfaces, but these will have more narrow constrictions than the first channel which appears at $\zeta = \zeta_c$, and as a first approximation we will neglect the contribution to the leak rate from these channels.

In the critical junction theory the leak rate is obtained by assuming that all the leakage occurs through the critical percolation channel and that the whole pressure drop $\Delta P = P_a - P_b$ occurs over the critical constriction (of length (in the fluid flow direction) λ_x and width λ_y, with $\lambda_x = \lambda_y = \lambda_c \approx L/\zeta_c$ and height $u_c = u_1(\zeta_c)$). Thus, for an incompressible Newtonian fluid, the volume-flow per unit time through the critical constriction will be (Poiseuille flow)

$$\dot{Q} \approx \frac{u_c^3}{12\eta}\Delta P, \tag{79}$$

where η is the fluid viscosity. For a rectangular nominal rubber-countersurface there is an additional factor L_y/L_x in (79), where L_x is the length (in the direction of fluid flow) and L_y is the width of the nominal contact region. Typically $L_y/L_x \gg 1$.

To complete the theory we must calculate the separation u_c of the surfaces at the critical constriction. We first determine the critical magnification ζ_c by assuming that the apparent relative contact area at this point (where the non-contact area percolates) is given by the Bruggeman effective medium theory: $A(\zeta_c)/A_0 = 0.5$. Knowing the critical magnification ζ_c, the separation $u_c = u_1(\zeta_c)$ at the critical junction can be obtained using the Persson contact mechanics theory.

The leak rate can also be expressed in terms of the flow factor ϕ_p. First note that the ensemble averaged current in the x direction $\bar{J}_x = -(\bar{u}^3\phi_p/12\eta)\,\mathrm{d}\bar{p}/\mathrm{d}x$ or since $\mathrm{d}\bar{p}/\mathrm{d}x = -\Delta P/L$ we get the leak rate

$$\dot{Q} = \bar{J}_x L = \frac{\bar{u}^3}{12\eta}\phi_p \Delta P. \tag{80}$$

Thus, ϕ_p can be determined from the leak rate $\dot{Q}$ if the average surface separation $\bar{u}$ is known. In the calculations presented below we have used the effective medium theory for the leak rate of seals. For high squeezing pressures this latter theory gives almost the same result as the critical junction theory [18], but for small contact pressures the effective medium theory is more accurate, and in fact for very small contact pressures it gives the same result for $\phi_p(\bar{u})$ (where $\bar{u}$ is the average interfacial separation) as predicted by the Tripp theory (which is exact to order $h_{rms}^2/\bar{u}^2$).

Figure 9 shows the logarithm (with 10 as the base) of the leak rate as a function of the logarithm of the squeezing pressured for a $d = 10$ μm thick Teflon film on top of a semi-infinite rubber block. The results are again for the power spectra **a** and **b** in figure 4 and for the (Teflon) laminated rubber (solid lines) and for pure rubber (dashed lines). The fluid viscosity $\eta = 0.001$ Pa s, the fluid pressure drop $\Delta P = 0.1$ MPa and the ratio $L_x/L_y = 16$. Note that the Teflon film for most squeezing pressures increases the leak rate by many orders of magnitude. Note also that, as the squeezing pressure goes toward zero, the leak rate for the laminated and pure rubber seals approach each other, which is expected because for low contact pressure the long-wavelength λ roughness will determine the leak rate and the contact mechanics at large length scales ($\lambda \gg d$) is not dependent on the stiff coating.

The fluid flow factor $\phi_p(\bar{u})$ for homogeneous bodies with isotropic surface roughness is a monotonically increasing function of $\bar{u}$. However, this is not always the case for layered materials. Thus, in figure 10 we show the pressure flow factor ϕ_p as a function of the average interfacial separation for a

$d = 10$ μm thick Teflon film on top of a semi-infinite rubber block. The results are for the power spectra **a** and **b** in figure 4. The origin of the non-monotonic dependence of $\phi_p(\bar{u})$ on $\bar{u}$ for surface **a** can be understood as follows.

For very large separation $\bar{u}$ (or low nominal contact pressures) the long-wavelength roughness will determine the flow factor and, with respect to the long-wavelength roughness, the layered material will deform as if the stiff top layer would not exist, and $\phi_p(\bar{u})$ will increase with increasing $\bar{u}/h_{rms}$ as expected for a homogeneous solid with the bulk (rubber) elastic properties. Note that the rms roughness h_{rms} is dominated by the long-wavelength contribution. As we increase the applied stress, $\bar{u}$ will decrease and the elastic solid will deform and follow the long-wavelength roughness down to a point where the wavelength becomes of the order of the thickness of the Teflon coating. From here on the contact area and the interfacial separation is mainly determined by the Teflon film, but now the relevant surface roughness is only the wavelength component smaller than the thickness of the film. Thus, with respect to the contact mechanics for small $\bar{u}$ the surface roughness h_{rms}^{eff} appears much smaller than the full roughness h_{rms}. This implies that for small $\bar{u}$ the flow factor will increase with $\bar{u}$ at a rate much higher than at large $\bar{u}$. This explains the general form of curve **a** in figure 10. For surface **b** there is almost no long-wavelength roughness and the flow factor (and leak rate) is determined mainly by the Teflon layer for all $\bar{u}$ and this explains why the flow factor in this case takes its usual form, being a monotonically increasing function of $\bar{u}$.

To summarize, the fluid flow factor for a homogeneous and isotropic material is a monotonically increasing function u/h_{rms}. In the case of layered materials, below a certain threshold of $\bar{u}$ the flow factor will be depend on the ratio $\bar{u}/h_{rms}^{eff}$ and since h_{rms}^{eff} is much smaller than h_{hrm} this means that $\bar{u}/h_{rms}^{eff} \gg \bar{u}/h_{rms}$ and therefore the flow factor will take almost the same value that it would take in the case of a homogeneous and isotropic material at much higher values of $\bar{u}/h_{rms}$. This explains the non-monotonic behavior of the curve.

6. Summary and conclusion

We have applied the contact mechanics model of Persson to layered materials. We have derived the M function, which relates the surface stress to the surface displacement, for a layered material, where the top layer (thickness d) has different elastic properties than the semi-infinite solid below. The formalism is valid for viscoelastic solids but is applied in this paper only to elastic materials. We have presented numerical results for the contact area as a function of the magnification for several different cases. For small magnifications, where only the long-wavelength roughness is observed, the contact mechanics does not depend on the thin-film coating. For very large magnification the contact area is the same as if the coating film would be infinitely thick. The transition from bulk to surface film dominance occurs at the magnification where the roughness wavelength of the order of the thickness of the film can first be observed.

We have also studied the dependence of the contact area on the Poisson ratio and plastic yield stress. We find that changing the Poisson ratio for the coating material from 0.5 (Teflon) to 0.3 (lower limit for polymer coatings) has a very small influence on the contact area. When plastic yielding is included in the analysis, the surfaces deform elastically with respect to the long-wavelength roughness (low magnification) but plastically at high enough magnification (involving shorter wavelength roughness).

As an application, we have studied the fluid leak rate for laminated rubber seals with Teflon-like coating. The large stiffness of the coating film as compared to the rubber bulk material underneath results in larger interfacial separation and larger leak rate as compared to the uncoated rubber seal. In most cases the critical junction, which determines most of the leakage, is observed at a magnification where negligible plastic deformation has occurred. As a result, in most cases it is not necessary to include plastic deformation when estimating the leak rate, even for coating materials like Teflon with a relatively low yield stress or penetration hardness. Finally, we have shown that for layered materials the fluid pressure flow factor ϕ_p may be a non-monotonic function of the average interfacial separation, in contrast to homogeneous materials with isotropic roughness for which ϕ_p increases monotonically with increasing $\bar{u}$.

Acknowledgments

I thank G Carbone for useful discussions. This work, as part of the European Science Foundation EUROCORES Program FANAS, was supported from funds by the DFG and the EC Sixth Framework Program, under contract no. ERAS-CT-2003-980409.

References

[1] Bhushan B and Peng W 2002 *Appl. Mech. Rev.* **55** 435
[2] Baek D K and Khonsari M M 2005 *Wear* **258** 898
[3] www.sitech-corp.com/abrasion/
[4] Brady R F 2001 *Prog. Org. Coat.* **43** 188
[5] Persson B N J 2001 *J. Chem. Phys.* **115** 3840
[6] Persson B N J 2006 *Surf. Sci. Rep.* **61** 201
[7] Persson B N J 2002 *Eur. Phys. J.* E **8** 385
[8] Bufler H 1971 *J. Elast.* **1** 125
[9] Burminster D M 1945 *J. Appl. Phys.* **16** 89
[10] Li J and Chou T W 1997 *Int. J. Solids Struct.* **34** 4463
[11] Nogi T and Kato T 1997 *ASME J. Tribol.* **119** 493
[12] O'Sullivan T C and King R B 1988 *J. Tribol.* **110** 235
[13] Campana C, Persson B N J and Müser M 2011 *J. Phys.: Condens. Matter* **23** 085001
[14] Carbone G and Mangialardi L 2008 *J. Mech. Phys. Solids* **56** 684
[15] Carbone1 G, Lorenz B, Persson B N J and Wohlers A 2009 *Eur. Phys. J.* E **29** 275–84
[16] Lorens B and Persson B N J 2010 *Eur. Phys. J.* **E31** 159
[17] Persson B N J and Yang C 2008 *J. Phys.: Condens. Matter* **20** 315011
[18] Persson B N J, Prodanov N, Krick B A, Rodriguez N, Mulakaluri N, Sawyer W G and Mangiagalli P 2012 *Eur. Phys. J.* E **35** 5